3-2018

Development of a semigraphitic sulfur-doped ordered mesoporous carbon material for electroanalytical applications

Jaqueline R. Maluta
University of São Paulo

Sergio A.S. Machado
University of São Paulo

Umesh Chaudhary
Iowa State University and Ames Laboratory

J. Sebastian Manzano
Iowa State University and Ames Laboratory, smanzano@iastate.edu

Lauro T. Kubota
Institute of Chemistry – UNICAMP

See next page for additional authors

Development of a semigraphitic sulfur-doped ordered mesoporous carbon material for electroanalytical applications

Abstract
The modification of traditional electrodes with mesoporous carbons is a promising strategy to produce high performance electrodes for electrochemical sensing. The high surface area of mesoporous carbons provides a large number of electroactive sites for binding analytes. Controlling the pore size and structure of mesoporous carbons and modifying their electronic properties via doping offers additional benefits like maximizing transport and tuning the electrochemical processes associated with analyte detection. This work reports a facile method to produce sulfur-doped ordered mesoporous carbon materials (S-OMC) with uniform pore structure, large pore volume, high surface area and semigraphitic structure. The synthesis used thiophenol as a single source of carbon and sulfur, and iron as a catalyst for low temperature carbonization. The S-OMC material was deposited on a glassy carbon electrode and used as a sensor with high sensitivity (11.7 A L mol−1) and selectivity for chloramphenicol detection in presence of other antibiotics. As a proof-of-concept, the sensor was applied to the direct analysis of the drug in reconstituted powdered milk and in commercial eye drops.

Keywords
Ordered mesoporous carbon, Sulfur-doped carbon, Mesoporous silica nanoparticles, Electrochemical sensor, Chloramphenicol detection

Disciplines
Materials Chemistry | Nanoscience and Nanotechnology | Physical Chemistry

Authors
Jaqueline R. Maluta, Sergio A.S. Machado, Umesh Chaudhary, J. Sebastian Manzano, Lauro T. Kubota, and Igor I. Slowing

Development of a semigraphitic sulfur-doped ordered mesoporous carbon material for electroanalytical applications

Jaqueline R. Maluta,[a] Sergio A. S. Machado,[a] Umesh Chaudhary,[b] J. Sebastián Manzano,[b] Lauro T. Kubota,[c] Igor I. Slowing[b*]

[a] São Carlos Institute of Chemistry, University of São Paulo, CP 380, CEP 13566-590, São Carlos, São Paulo, Brazil

[b] US DOE Ames Laboratory and Department of Chemistry, Iowa State University, Ames, Iowa, 50011, United States

[c] Department of Analytical Chemistry, Institute of Chemistry – UNICAMP, P.O. Box 6154, 13084-971, Campinas, SP, Brazil

*Corresponding author:

E-mail address: islowing@iastate.edu

Highlights

- Thiophenol as a new source to produce S-doped ordered mesoporous carbons (S-OMC).
- Iron in silica template catalyzes low temperature carbonization in S-OMC synthesis.
- Fast electron transfer and conductivity make S-OMC suitable to produce electrodes.
- S-OMC modified GC electrodes display ppb sensitivity for selective CAP detection.
- S-OMC/GC electrodes quantify CAP in powdered milk without any sample preparation.

Graphical abstract

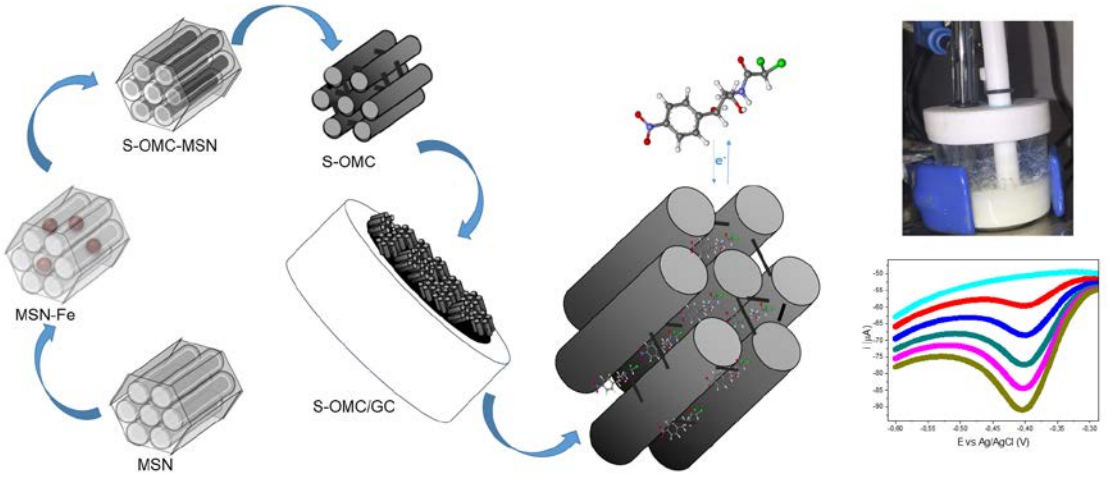

Abstract

A promising strategy to produce high performance electrodes for electrochemical sensing is the modification of traditional electrodes with mesoporous carbons. The high surface area of these materials provides a large number of electroactive sites for binding analytes. Controlling the pore size and structure of mesoporous carbons and modifying their electronic properties via doping offers additional benefits like maximizing transport and tuning the electrochemical processes associated with analyte detection. This work reports a facile method to produce sulfur-doped ordered mesoporous carbon materials (S-OMC) with uniform pore structure, large pore volume, high surface area and semigraphitic structure. The synthesis uses thiophenol as the single source of carbon and sulfur, and iron as catalyst for low temperature carbonization. The S-OMC material was assembled on a glassy carbon electrode and used as a sensor with excellent sensitivity (18.9 $A \cdot L \cdot mol^{-1}$) and selectivity for chloramphenicol detection in presence of other antibiotics. The sensor was successfully used for direct analysis of the drug in milk without requiring any sample preparation.

Keywords: ordered mesoporous carbon, sulfur-doped carbon, mesoporous silica nanoparticles, electrochemical sensor, chloramphenicol detection

1. Introduction

Several different carbon materials are used in electroanalysis due to their electrical conductivity, chemical inertness, and low background current.[1] Nanostructured carbons such as ordered mesoporous carbons (OMC) have the additional benefits of uniform pore structures, large pore volumes, high specific surface areas, and tunable pore size distributions, which can maximize the interaction with analytes and ensure fast mass transport.[2, 3] Furthermore, due to their fast electron transfer capacity and excellent electrocatalytic activity, OMC have been recently used in sensing,[4] with excellent performance in detection of morphine, epinephrine, acetaminophen, H_2O_2, nitrobenzene, and NADH.[5-7] The superb electrochemical behavior of OMC may be attributed to a large number of edge plane defect sites on their accessible surface.[6]

OMC are typically synthesized by infiltration of the pores of a mesoporous silica template with appropriate carbon precursor, followed by carbonization, and subsequent template removal.[8] The graphitic character of OMC determines its electrical conductivity, and is key for its electrochemical applications.[9] A high graphitic character and electrical conductivity can be achieved by using aromatic precursors,[10] carbonizing at high pressures,[11] chemical vapor deposition,[12] or addition of iron as carbonization catalyst.[13, 14]

The electronic properties of OMC can be controlled by incorporating heteroatoms into their structure. While nitrogen doping of OMC has been widely explored,[15] sulfur doping is less common. S-doped OMC (S-OMC) have been obtained by post-synthesis treatment using melt-diffusion,[16-18] or directly synthetized using sulfur-containing molecules like p-toluenesulfonic acid or benzyl disulfide as carbon source.[19-21] These S-doped materials have been used to promote metal-support interactions in the catalytic oxygen reduction reaction,[21] and in the adsorption of acetaminophen,[22, 23] oxygen,[24, 25] and dibenzothiophene.[26, 27]

Chloramphenicol (CAP) is a broad-spectrum antimicrobial with remarkable antibacterial and pharmacokinetic properties. However, this drug is considered an environmental contaminant and is forbidden for use in food-producing animals[28, 29] because it is associated with human health issues such as aplastic anemia, hepatic dysfunction, gray syndrome, and cancer.[30, 31] In spite of this status, the Rapid Alert

System for Food and Feed (RASFF) of the European Union has reported over 80 notifications of the illegal use of CAP between 2010 and 2017.[32] Therefore, the detection of this drug has financial, environmental, and public health importance. Herein, we report the synthesis and characterization of an S-OMC with semi-graphitic character prepared using thiophenol as an aromatic S-containing carbon precursor and iron as a catalyst. Because of its adsorptive and electrochemical properties, the material was used to assemble modified electrodes for the direct detection and quantification of ppb levels of CAP.

2. Materials and methods

2.1 Preparation of S-OMC

SBA-15 type mesoporous silica nanoparticles (MSN) were synthetized following previous reports.[33] Briefly, 7.0 g of Pluronic P-104 was dissolved in 164 mL of Millipore water and 109 mL of HCl 4.0 M. The resulting solution was stirred for 1 h at 52 °C. Then, 10.64 g of TMOS was added and the solution was stirred for further 24 h at 52 °C. After this, the solution was placed in an autoclave for hydrothermal treatment at 150 °C for additional 24 h. The MSN product was then filtered, washed with ethanol and dried in air. The surfactant was removed by calcination in air at 550 °C for 6 h. Following a literature procedure, [3, 10] a solution of $Fe(NO_3)_3 \cdot 9H_2O$ (0.382 g, 0.764 g, or 1.145 g) in acetone (1 mL) was impregnated into the MSN (1.0 g), and calcined in air at 350 °C for 6 h. Finally, the ordered mesoporous carbon (OMC) was synthesized by impregnating 1.0 g of Fe-MSN composite with 9 mmol of thiophenol, drying at 70 °C and carbonizing at 600 °C or 900° C during 7 h under flowing Ar. The silica template was removed by refluxing in a water:ethanol (1:1) solution of NaOH (1 M) overnight at 80 °C (twice). The resulting S-OMC material was filtered out, washed with Millipore water and dried in air at 70 °C.

2.2 Characterization

Wide and low angle X-ray diffraction (XRD) patterns were acquired using a Shimadzu XRR7000 and a BRUKER APEX II Duo, respectively. Both diffractometers used Cu Kα (λ=1.5405Å) radiation source operating at 40 kV and 30 mA. Raman spectra were acquired on a confocal Horiba Scientific T64000 Raman spectrometer using a 633 nm laser as the excitation source. The powdered materials were directly analyzed by infrared

spectroscopy in Attenuated Total Reflectance mode (IR-ATR) using a Bruker Vertex80 FT-IR spectrometer. The surface area and porosity were measured by nitrogen sorption isotherms at 196 °C in a Micromeritics TriStar instrument after a 6 h pre-treatment at 100 °C under N_2 flow. The surface area was calculated by Brunauer-Emmett-Teller (BET) methodology and the pore size distribution by Barret-Joyner-Halenda (BJH). Scanning electron microscopy was performed with a JEOL JSM634 F equipped with Field Emission Gun (SEM-FEG). Electron diffraction spectrometry (EDS) was realized at Eletronic Microscopy ZEISS LEO 440 (Cambridge, England) linked with EDX LINK ANALYTICAL, (Isis System Series 300) detector. Transmission electron microscopy (TEM) was performed with LIBRA120 microscope.

2.3 Electrochemical measurements

The electrochemical measurements were performed in an AUTOLAB PGSTAT 12, interfaced with NOVA software, using a three-electrode cell. Ag/AgCl (3M KCl) and Pt foil (1 cm^2) were used as reference and counter electrode respectively. As working electrode, a glassy carbon (GC) electrode (3 mm diameter), was polished with alumina and rinsed thoroughly with doubly distilled water. Then, 10 μL of the respective S-OMC dispersion (2.0 ± 0.05 mg S-OMC in 1 mL DMF) was drop casted onto the surface of the GC electrode and dried to obtain an S-OMC/GC modified electrode. The electrolyte was bubbled with N_2 to remove O_2 before the experiments.

3. Results and discussion

3.1 S-OMC synthesis

Iron is a well-known carbon polymerization catalyst,[34, 35] therefore it was used to promote the OMC synthesis (Scheme 1). Impregnation of $Fe(NO_3)_3 \cdot 9H_2O$ (0.382 g, 0.95 mmol) on SBA-15 type mesoporous silica nanoparticles (MSN) (1.0 g) followed by calcination led to a small decrease in the surface area and pore volume of the material (Table 1). SEM imaging of the composite showed no evidence of free iron oxide particles around or on the external surface of MSN, however EDS analysis indicated Fe was present on the template at 1.9 atom % (Table 1, Fig. S1) suggesting the metal was located inside the

mesopores, which is consistent with the ca. 10% decrease in pore volume of the material. Impregnation of the Fe-MSN composite with thiophenol followed by carbonization at 600 °C produced a black material (Fig. 1A, left). In contrast, impregnation of iron-free MSN with thiophenol and carbonization at 600 °C led to a gray material suggesting low carbonization efficiency in absence of the metal (Fig. 1A, right). EDS analysis of the carbonized thiophenol-Fe-MSN composite revealed a homogeneous distribution of C (ca. 50 atom %) and S (ca. 1 atom %) over different areas of the material (Table S1).

Scheme 1: Steps of S-OMC synthesis.

Dissolution of the silica template from the composite in aqueous NaOH yielded a S-OMC material with well-defined mesopore structure evidenced by TEM imaging, indicating successful replication of the cylindrical channels of the MSN template (Fig. 1B). Low angle powder XRD further confirmed the structural relation to the parent MSN showing a sharp reflection at 0.6 2θ degrees associated to the (100) plane of a 2D hexagonal structure (Fig. 1C). Nitrogen sorption analysis of the S-OMC indicated a type IV isotherm (Fig. 1d) characteristic of a mesoporous material with narrow pore width distribution[36] centered at 4.8 nm. Interestingly, the surface area of S-OMC was significantly larger (ca. 150 %) than the parent MSN (Table 1), likely due to the lower density of the carbon material. Carbonization at higher temperature (900 °C) led to a drop in surface area, pore volume, and pore width. Subtracting the pore width from the mesopore unit cell parameter a_0 ($a_0 = (2/\sqrt{3})d_{100}$) indicated that the higher carbonization temperature led to thicker pore walls (11.4 nm at 600 °C versus 13.5 nm at 900 °C) and shrinking of the structure, likely due to cross-linking of poly(phenylene sulfide) via formation of S-heterocycles during carbonization.[37] Increasing the amount of iron in the synthesis also led to smaller surface areas, pore volumes and pore widths (Table S2).

Table 1: Textural properties and chemical composition of the materials.

	SA_{BET} [a] (m^2/g)	V_{BJH} [b] (cm^3/g)	w_{BJH} [c] (nm)	C [d] (at %)	O [d] (at %)	Si [d] (at %)	S [d] (at %)	Fe [d] (at %)
MSN	400	0.97	7.4	-	67.0±1.5	33.0±1.5	-	-
Fe-MSN	385	0.87	7.3	-	61.0±6.5	37.1±6.3	-	1.9±0.3
S-OMC_{600}	596	0.82	4.8	79.8±2.0	15.9±1.8	2.4±0.9	1.5±0.7	0.5±0.1
S-OMC_{900}	388	0.39	3.7	67.2±1.3	27.1±1.3	3.8±0.1	0.5±0.1	1.5±0.1

[a] Surface area calculated by Brunauer-Emmett-Teller method.
[b] Pore volume calculated by Barret-Joyner-Halenda method.
[c] Average pore width calculated by Barret-Joyner-Halenda method.
[d] Obtained from energy dispersive x-ray spectroscopy.

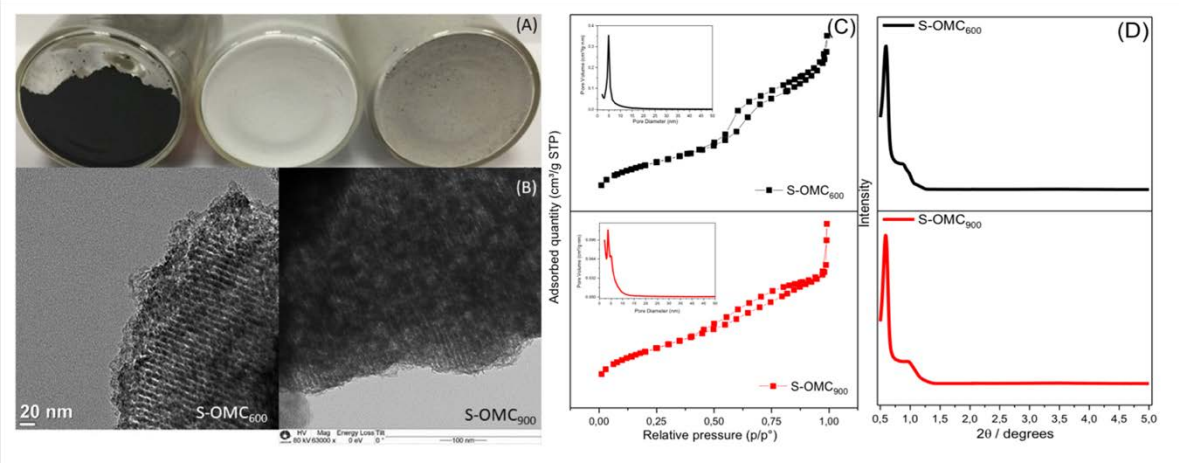

Fig. 1. (A) Carbonized thiophenol-MSN composites with (left) and without (right) iron, and original MSN (middle) for comparison: the gray color of the material without iron suggests incomplete carbonization as opposed to the black carbonized iron-containing material. (B) TEM images, (C) N_2 sorption isotherms and pore size distributions (inset), and (D) small-angle X-ray diffraction patterns of S-OMC carbonized at 600 °C and 900 ºC.

Wide angle XRD analysis of the S-OMC carbonized at 600 °C (S-OMC_{600}) revealed two broad reflections at 23.5 and 44.1 2Θ degrees that were indexed as d_{002} and d_{101} interlayer spacings of carbon planes (Fig. S2A). Both peaks were slightly shifted (26.1 and 42.8) and better defined in the S-OMC carbonized at 900 °C (S-OMC_{900}) indicating

decreasing d-spacings and increasing degree of graphitization with carbonization temperature. The d_{002} interlayer spacing of S-OMC$_{900}$ (0.341 nm) is between typical values for turbostratic (0.344 nm) and graphitic carbon (0.335 nm).[38, 39] Reflections attributable to iron oxides were only observed at higher iron loadings, and they appear to be related to magnetite (Fig. S3).[40] In fact, all the OMCs were attracted to magnets.

Raman spectroscopy of S-OMC$_{600}$ and S-OMC$_{900}$ showed the characteristic D (1300 cm^{-1}) and G (1590 cm^{-1}) bands of sp^2 carbon layers (Fig. S2B).[41] Because both materials show I_D/I_G ratios larger than 1, the polycyclic aromatic layers should be largely disordered, yet S-OMC$_{900}$ showed a smaller I_D/I_G ratio (1.36) than S-OMC$_{600}$ (1.63), indicating increasing order (i.e. graphitic character) at higher carbonization temperatures, which is consistent with the XRD data. Increasing the amount of iron in S-OMC$_{600}$ material also led to lower I_D/I_G ratios (i.e. improved graphitic character, Fig. S3B,C) further confirming that iron promotes carbon graphitization. While XRD and Raman data indicate a more graphitic character of S-OMC$_{900}$ than S-OMC$_{600}$, the S content is significantly lower in the former.

3.2 Electrochemical properties of S-OMC

To study the electrochemical behavior of S-OMC the materials were suspended in DMF, drop casted on clean glassy carbon (GC) electrodes, and dried. Investigation of the modified electrode/electrolyte interface was carried out by cyclic voltammetry (CV) of $[Fe(CN)_6]^{3-/4-}$ (10 mM) from -0.5 to 1 V with KCl electrolyte (0.1 mM) at a 100 mV s^{-1} scan rate. The cyclic voltammograms obtained using S-OMC$_{600}$ and S-OMC$_{900}$ modified glassy carbon (S-OMC/GC) electrodes were acquired in absence and presence of 10 mM $[Fe(CN)_6]^{3-/4-}$ (Fig. 2). The $[Fe(CN)_6]^{3-/4-}$ redox cycle gave faster electron transfer rates and higher peak currents on S-OMC$_{900}$ (ΔE = 116 mV, 132 µA/-133 µA) than S-OMC$_{600}$ (ΔE = 144 mV, 107µA/-114 µA) modified GC electrodes. These differences indicate that in spite of its smaller surface area S-OMC$_{900}$ is more electroactive than S-OMC$_{600}$, likely due to the higher conductivity that results from the increased graphitic character and smaller d-spacing of the former.

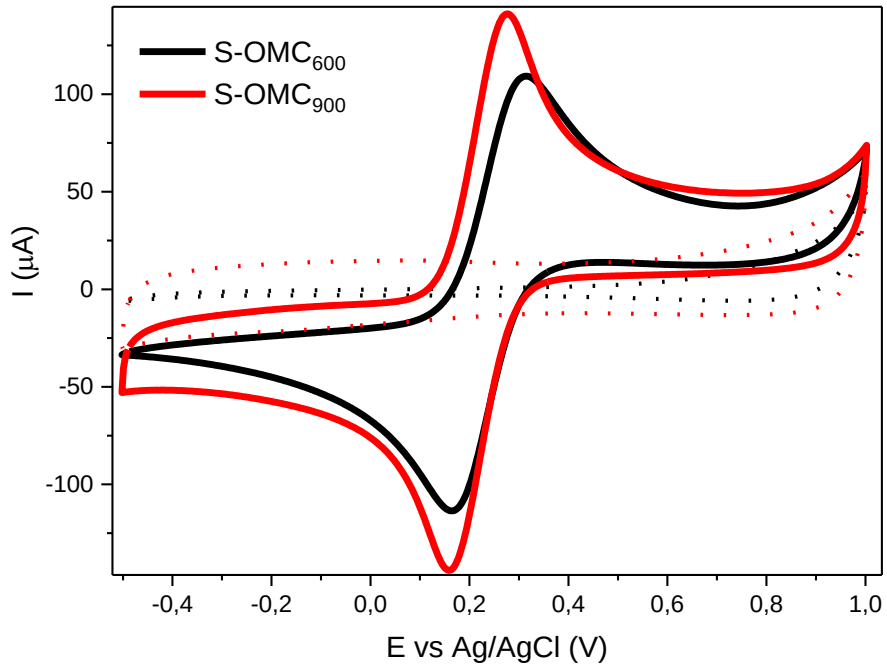

Fig. 2. Cyclic voltammogram in absence (····) and presence (—) of 10 mM $[Fe(CN)_6]^{3-/4-}$ in 0.1 mM KCl using GC, S-OMC$_{600}$/GC or S-OMC$_{900}$/GC as working electrode.

3.3 Application of S-OMC/GC as chloramphenicol sensors

As a proof-of-concept, the two S-OMC/GC electrodes were then used to examine the electrochemical behavior of chloramphenicol (CAP) solutions. The cyclic voltammograms of CAP (3 mM) on S-OMC$_{600}$/GC and S-OMC$_{900}$/GC in 0.1 M H_2SO_4, presented well-defined cathodic and anodic peaks attributed to redox transformations of the nitro group (Fig. 3).[42] The peak currents obtained with the S-OMC modified electrodes were higher and appeared at lower potentials than with the bare GC electrode. The cathodic peak appeared at a more negative potential for S-OMC$_{600}$/GC (-343 mV) than S-OMC$_{900}$/GC (-270 mV), and was attributed to the irreversible reduction of the nitro group to hydroxylamine (Equation 1) based on literature reports.[43, 44] The 73 mV reduction underpotential and fourfold peak current enhancement observed for S-OMC$_{900}$/GC relative to S-OMC$_{600}$/GC indicated the former is a more efficient electrocatalyst for the reduction of the nitro group in CAP than the latter. This behavior is consistent with the results obtained from the cyclic voltammetry of $Fe(CN)_6^{-4/-3}$, and can therefore be attributed to the increased graphitic character of S-OMC$_{900}$. Interestingly, while the voltammograms of the

reaction using S-OMC$_{600}$/GC presented two additional well-defined redox peaks (E_R= 307 mV; E_O= 340 mV) associated with the reversible interconversion of the hydroxylamine and nitroso states (Equation 2),[43, 44] these peaks were significantly less evident when using S-OMC$_{900}$/GC, suggesting lower adsorption of the hydroxylamine intermediate onto S-OMC$_{900}$ than S-OMC$_{600}$.

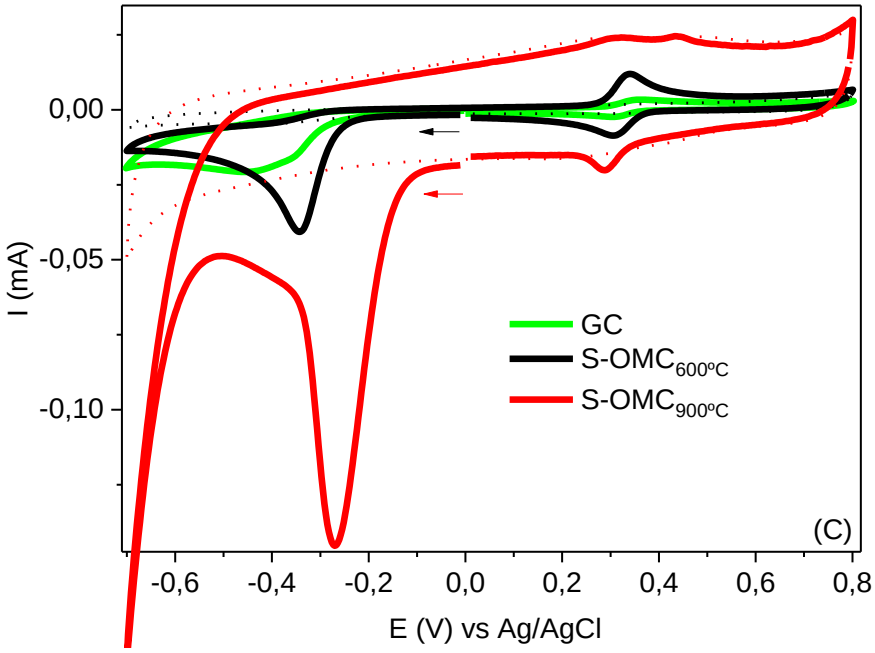

Fig. 3. Cyclic voltammogram in absence (····) and presence (—) of 3 mM chloramphenicol in 0.1 M H_2SO_4 as electrolyte, using GC, S-OMC$_{600}$/GC or S-OMC$_{900}$/GC as working electrode.

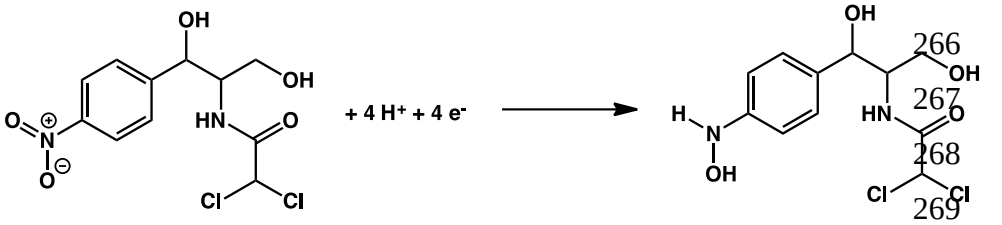

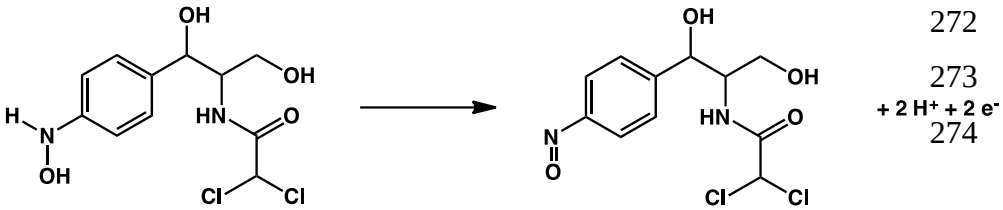

The effect of scan rate on the cathodic peak current (-270 mV) was investigated to obtain more insights into the mechanism of the electrochemical reduction of the nitro group of CAP (Fig. S4). A linear correlation ($R^2 = 0.999$) between the cathodic peak current and the scan rate was found in the range of 50-400 mV s^{-1}, suggesting an adsorption-controlled process.[45] This behavior indicates that the high surface area of the S-OMC materials is critical to their electrochemical performance. Furthermore, the open mesoporous structure and large pore volume of S-OMC are key to maximize the accessibility of small molecules to the electrochemically active surface, and allow loading large amounts of the target molecules (on the order of mmol g^{-1}).[2, 46] This result suggested that including a pre-concentration step should increase the capacity of detecting CAP with S-OMC/GC. To explore this possibility, a linear sweep voltammetry (LSV) of CAP (3 mM in 0.1 M H_2SO_4) was performed using S-OMC_{900}/GC as the work electrode with open circuit pre-accumulation steps of variable times. The results indicated that the peak current increased with pre-accumulation time in the range of 0 to 360 s, but no further increase was observed at longer times (Fig. S5). Therefore, a 360 s pre-accumulation step was applied to all of the following experiments.

The effect of acidity on the behavior of the electrochemical reduction of CAP, was investigated using phosphate buffered saline (PBS) solutions at pH varying from 1.9 to 10.4 (Fig. S6). The peak potential shifted linearly (R^2=0.997) with pH to increasingly negative values, indicating the participation of H^+ in the reaction, which is consistent with Equation (1).[47] Because of the small underpotential in acid electrolytes, a 0.1M H_2SO_4 solution was used to prepare a calibration curve for the quantification of the drug (Fig. 4). The reduction peak current (-270 mV) increased linearly ($R^2 = 0.995$) with chloramphenicol concentration (5 to 10 µmol · L^{-1}) following the regression equation $i = 1.4 \times 10^{-6} + 10.5c$ (i = current in A and c = concentration in mol · L^{-1}) with a sensitivity of 10.5 A · L · mol^{-1}. At lower concentrations (0.1 to 0.25 µmol · L^{-1}), a better sensitivity was obtained (18.9 A · L · mol^{-1}) with good linearity ($R^2 = 0.997$) and regression equation $i = -9.3 \times 10^{-7} + 18.9c$. The limit of detection was calculated as 7.9×10^{-9} mol · L^{-1} (LOD = 3SD/S), and the limit of quantification was 2.6×10^{-8} mol · L^{-1} (LOQ = 10SD/S), were SD is the standard deviation of 10 blank measurements (5×10^{-8} A) and S is the curve slope (18.9 A · L · mol^{-1}). The

obtained values are comparable or better than other electrodes reported in the literature (Table S2), and highly repeatable, with a 2.3% relative standard deviation (RSD) for ten consecutive measurements (Fig. S7a). The reproducibility of preparation the S-OMC modified GC electrodes was estimated by comparing the performances of three freshly produced electrodes (Fig. S7b). The low RSD (1.8%) obtained for the peak reduction current measurements demonstrated a highly reproducible manufacturing method.

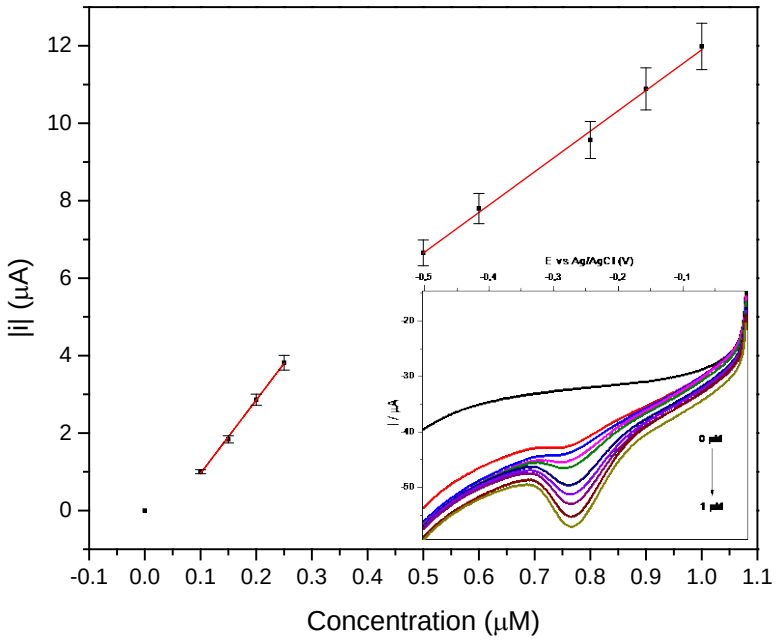

Fig. 4. Plots of reduction peak current intensity (-270 mV) versus chloramphenicol concentration. Insert: LSV plots using S-OMC$_{900}$/GC, in H_2SO_4 0.1 M in presence of increasing chloramphenicol concentrations (0.1, 0.15, 0.2, 0.25, 0.5, 0.6, 0.8, 0.9, 1 µmol · L^{-1}, respectively.)

To investigate the selectivity of the sensor, thiamphenicol (TAP) and florfenicol (FLF), two allowed antibiotics with structures similar to CAP (Fig. 5A-D), were analyzed as controls. Because ampicillin (AMP) is usually administered in association with CAP, its potential interference with the detection of the latter was also evaluated. Cyclic voltammetry experiments of TAP, FLF, AMP (1.5 mM each) and combinations thereof revealed no peak in the range 0 to -0.6 V, indicating none of the functionalities in these

antibiotics was reducible in the same regime as the nitro group in CAP (Fig. 5E). Addition of CAP (1.5 mM) to a mixture containing all of these antibiotics led to a dramatic increase in current, demonstrating that the method is selective.

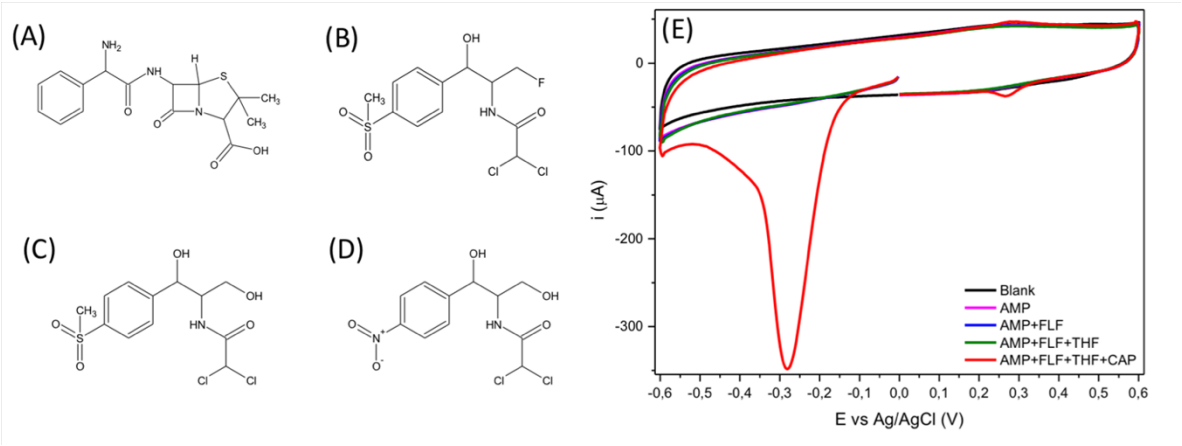

Fig. 5. Chemical structures of (A) ampicillin (AMP), (B) florfenicol (FLF), (C) thiamphenicol (THF), and (D) chloramphenicol (CAP); and cyclic voltammetry in absence and presence of ampicillin, florfenicol, thiamphenicol and chloramphenicol (1.5 mM each) in H_2SO_4 0.1M using S-OMC_{900C}/GC as working electrode.

Finally, the capacity of the S-OMC_{900}/GC electrode to detect and quantify CAP in commercial powdered milk was evaluated. The measurements were carried out using the standard addition method. For this, commercial powdered milk was dissolved in H_2SO_4 0.1M (1 g in 10 mL) and analyzed directly, without any further processing. The LSV of the reconstituted milk showed no interfering peaks at the detection potential. Upon addition of CAP in the 50 to 250 μmol L^{-1} concentration range, a linear analytical response (R^2 = 0.9996) was obtained with good sensitivity 0.11 A · L · mol^{-1} but two orders of magnitude smaller than the sensitivity in 0.1 M H_2SO_4, likely due to matrix interference. The limit of detection was calculated as 1.9×10^{-6} mol · L^{-1} (LOD = 3SD/S), and the limit of quantification was 6.3×10^{-6} mol · L^{-1} (LOQ = 10SD/S), were SD is the standard deviation of 10 blank measurements (7×10^{-8} A) and S is the curve slope (0.11 A · L · mol^{-1}). Because of this, the method of standard addition is well suited for the application of CV to the direct determination of CAP in milk, without any sample preparation.

4. Conclusions

Thiophenol was effectively used as a new carbon source for producing S-doped OMC with SBA-15 type mesoporous silica nanoparticles as a hard template. The process required iron to facilitate carbon formation, and the graphitic character increased with the amount of iron employed in the synthesis. Higher carbonization temperatures (900 °C) also led to increasing graphitic character. The S-OMC_{900} material was used to modify a glassy carbon electrode and presented a small charge transference resistance, high peak current and smaller underpotential in presence of the redox probe $[Fe(CN)_6]^{3-/4-}$. The modified electrode was applied, as proof-of-concept, as a selective CAP sensor. The highly ordered mesopores and large surface area and pore volume of S-OMC_{900}, allowed fast mass transport of CAP to ensure efficient interaction with the surface of the material. The semi-graphitic character of the material led to fast electron transfer rates, good conductivity and less resistive behavior for the electrochemical analysis. The LSV with 360 s pre-accumulation led to with good sensitivity for CAP detection and nanomolar LOD (7.9×10^{-9} mol L^{-1}). Also, the proposed methodology allows the direct detection of CAP in powdered milk, without any sample preparation.

Acknowledgments

The authors thank CAPES and CNPq for financial support, INCT/INOMAT – National Institute of Science, Technology and Innovation in Complex Functional Materials (CNPq-MCTI/Fapesp) for TEM images. U.C., J.S.M. and I.I.S. acknowledge funding support from the U.S. Department of Energy, Office of Basic Energy Sciences, Division of Chemical Sciences, Geosciences, and Biosciences through the Ames Laboratory. The Ames Laboratory is operated for the U.S. Department of Energy by Iowa State University under Contract No. DE-AC02-07CH11358.

References

[1] J.C. Ndamanisha, L.-P. Guo, Anal. Chim. Acta, 747 (2012) 19-28.
[2] A. Walcarius, Trends Anal. Chem., 38 (2012) 79-97.
[3] T.-W. Kim, P.-W. Chung, I.I. Slowing, M. Tsunoda, E.S. Yeung, V.S.-Y. Lin, Nano Lett., 8 (2008) 3724-3727.
[4] Y. Zhou, L. Tang, G. Zeng, J. Chen, Y. Cai, Y. Zhang, G. Yang, Y. Liu, C. Zhang, W. Tang, Biosens. Bioelectron., 61 (2014) 519-525.
[5] F. Li, J. Song, C. Shan, D. Gao, X. Xu, L. Niu, Biosens. Bioelectron., 25 (2010) 1408-1413.
[6] J.B.Raoof, F.Chekin, R.Ojani, S.Barari, M.Anbia, S.Mandegarzad, Anglais, 16 (2012) 8.
[7] Y. Zhang, X. Bo, A. Nsabimana, C. Luhana, G. Wang, H. Wang, M. Li, L. Guo, Biosens. Bioelectron., 53 (2014) 250-256.
[8] R. Ryoo, S.H. Joo, M. Kruk, M. Jaroniec, Adv. Mater., 13 (2001) 677-681.
[9] H. Chang, S.H. Joo, C. Pak, J. Mater. Chem., 17 (2007) 3078-3088.
[10] C.H. Kim, D.-K. Lee, T.J. Pinnavaia, Langmuir, 20 (2004) 5157-5159.
[11] T.-W. Kim, I.-S. Park, R. Ryoo, Angew. Chem., 115 (2003) 4511-4515.
[12] Y. Xia, R. Mokaya, Adv. Mater., 16 (2004) 1553-1558.
[13] W. Gao, Y. Wan, Y. Dou, D. Zhao, Adv. Energ. Mater., 1 (2011) 115-123.
[14] Z. Wu, Y. Yang, D. Gu, Y. Zhai, D. Feng, Q. Li, B. Tu, P.A. Webley, D.Y. Zhao, Top. Catal., 52 (2009) 12-26.
[15] R. Liu, D. Wu, X. Feng, K. Müllen, Angew. Chem., 122 (2010) 5.
[16] X.Liang, Z.Wen, Y.Liu, H.Zhang, L.Huang, J.Jin, J.PowerSourc.,196 (2011)3655-3658.
[17] H. Wang, C. Zhang, Z. Chen, H.K. Liu, Z. Guo, Carbon, 81 (2015) 782-787.
[18] S.-R. Chen, Y.-P. Zhai, G.-L. Xu, Y.-X. Jiang, D.-Y. Zhao, J.-T. Li, L. Huang, S.-G. Sun, Electrochim. Acta, 56 (2011) 9549-9555.
[19] H.I. Lee, S.H. Joo, J.H. Kim, D.J. You, J.M. Kim, J.-N. Park, H. Chang, C. Pak, J. Mater. Chem., 19 (2009) 5934-5939.
[20] K. Kwon, S.-a. Jin, C. Pak, H. Chang, S.H. Joo, H.I. Lee, J.H. Kim, J.M. Kim, Catal. Today, 164 (2011) 186-189.
[21] H. Wang, X. Bo, Y. Zhang, L. Guo, Electrochim. Acta, 108 (2013) 404-411.
[22] A.P.Terzyk, G.Rychlicki, Coll.Surf.A: Physicochem. Eng.Aspects, 163 (2000) 135-150.
[23] A.P. Terzyk, Coll. Surf. A: Physicochem. Eng. Aspects, 177 (2001) 23-45.
[24] M. Seredych, K. László, T.J. Bandosz, ChemCatChem, 7 (2015) 2924-2931.
[25] R. Yang, Y. Sun, Z. Yang, J. Wu, in: Meeting Abstracts, The Electrochemical Society, 2015, pp. 736-736.
[26] M. Seredych, T.J. Bandosz, Carbon, 49 (2011) 1216-1224.
[27] M. Seredych, M. Khine, T.J. Bandosz, ChemSusChem, 4 (2011) 139-147.
[28] T.L. Fodey, S.E. George, I.M. Traynor, P. Delahaut, D.G. Kennedy, C.T. Elliott, S.R.H. Crooks, J. Immunol. Methods, 393 (2013) 30-37.
[29] J. Ferguson, A. Baxter, P. Young, G. Kennedy, C. Elliott, S. Weigel, R. Gatermann, H. Ashwin, S. Stead, M. Sharman, Anal. Chim. Acta, 529 (2005) 109-113.
[30] F.T. Fraunfelder, G.C. Bagby, D.J. Kelly, Am. J. Ophthalmol., 93 (1982) 356-360.
[31] K. Krasinski, R. Perkin, J.C. Rutledge, Clin. Pediat., 21 (1982) 571-572.

[32] European Commission, RASFF Portal, https://webgate.ec.europa.eu/rasff-window/portal/?event=searchForm&cleanSearch=1 (accessed 10/05/2017).

[33] K. Kandel, U. Chaudhary, N.C. Nelson, I.I. Slowing, ACS Catal., 5 (2015) 6719-6723.
[34] W. Li, S. Xie, L. Qian, B. Chang, Science, 274 (1996) 1701.
[35] S. Li, G.D. Meitzner, E. Iglesia, J. Phys. Chem. B, 105 (2001) 5743-5750.
[36] J. Xu, Z. Luan, H. He, W. Zhou, L. Kevan, Chem. Mater., 10 (1998) 3690-3698.
[37] A. Oya, K. Arai, K. Fujita, J Mater Sci, 29 (1994) 4477-4480.
[38] G. Bacon, Acta Crystallogr., 4 (1951) 558-561.
[39] U. Rost, R. Muntean, P. Podleschny, G. Marginean, M. Brodmann, V.A. Şerban, in: Solid State Phenomena, Trans Tech Publ, 2016, pp. 27-32.
[40] X. Dong, H. Chen, W. Zhao, X. Li, J. Shi, Chem. Mater., 19 (2007) 3484-3490.
[41] F. Su, J. Zeng, X. Bao, Y. Yu, J.Y. Lee, X. Zhao, Chem. Mater., 17 (2005) 3960-3967.
[42] S. Chuanuwatanakul, O. Chailapakul, S. Motomizu, Anal. Sci., 24 (2008) 493-498.
[43] J. Borowiec, R. Wang, L. Zhu, J. Zhang, Electrochim. Acta, 99 (2013) 138-144.
[44] H. Zhao, Y. Chen, J. Tian, H. Yu, X. Quan, J. Electrochem. Soc., 159 (2012) 6.
[45] D. Zheng, J. Ye, L. Zhou, Y. Zhang, C. Yu, J. Electroanal. Chem., 625 (2009) 82-87.
[46] J. Zang, C.X. Guo, F. Hu, L. Yu, C.M. Li, Anal. Chim. Acta, 683 (2011) 187-191.
[47] M. Zhou, L.-P. Guo, Y. Hou, X.-J. Peng, Electrochim. Acta, 53 (2008) 4176-4184.
[48] H. Alemu, L. Hlalele, Bull. Chem. Soc. Ethiopia, 21 (2007).
[49] T. Alizadeh, M.R. Ganjali, M. Zare, P. Norouzi, Food Chem., 130 (2012) 1108-1114.
[50] X. Zhang, Y.-C. Zhang, J.-W. Zhang, Talanta, 161 (2016) 567-573.
[51] L. Agüí, A. Guzmán, P. Yáñez-Sedeño, J.M. Pingarrón, Anal. Chim. Acta, 461 (2002) 65-73.
[52] M.L. Mena, L. Agüí, P. Martinez-Ruiz, P. Yáñez-Sedeño, A.J. Reviejo, J.M. Pingarrón, Anal. Bioanal. Chem., 376 (2003) 18-25.
[53] F.-Y. Kong, T.-T. Chen, J.-Y. Wang, H.-L. Fang, D.-H. Fan, W. Wang, Sens. Actuators B Chem., 225 (2016) 298-304.
[54] M. Zhu, Y. Zhang, J. Ye, H. Du, Int. J. Electrochem. Sci., 10 (2015) 8263-8275.

Supplementary material

Development of a semigraphitic sulfur-doped ordered mesoporous carbon material for electroanalytical applications

Jaqueline R Maluta[A], Sergio A S Machado[A], Umesh Chaudhary[B], J. Sebastián Manzano[B], Lauro T Kubota[C], Igor I. Slowing[B,*]

[A] São Carlos Institute of Chemistry, University of São Paulo, CP 380, CEP 13566-590, São Carlos, São Paulo, Brazil

[B] Ames Laboratory and Department of Chemistry, Iowa State University, Ames, Iowa 50011, United States

[C] Department of Analytical Chemistry, Institute of Chemistry – UNICAMP, P.O. Box 6154, 13084-971, Campinas, SP, Brazil

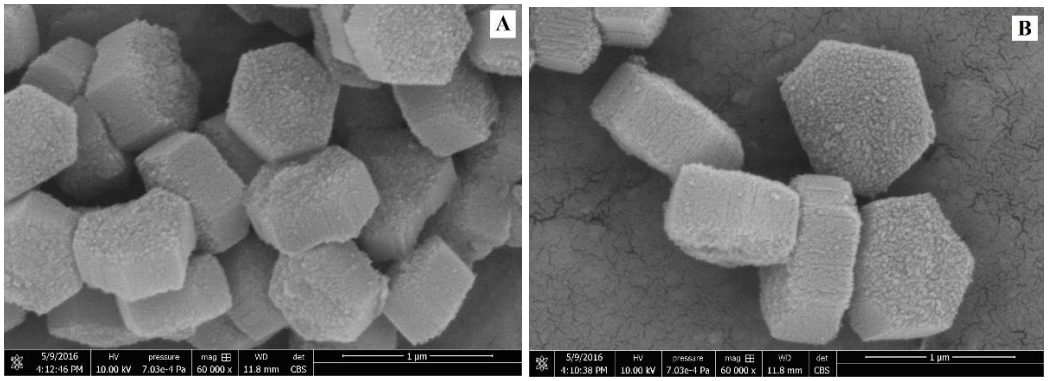

Fig. S1. SEM-FEG-DBS images of the (A) SBA-15 type MSN and (B) Fe-MSN composite.

Table S1. Chemical composition by EDS of the thiophenol-Fe-MSN material carbonized at 600 °C.

	Area 1	Area 2
C	49.01	51.03
O	37.68	36.72
Si	11.55	10.48
S	1.05	1.12
Fe	0.71	0.64
C/Si	4.3	4.9

480

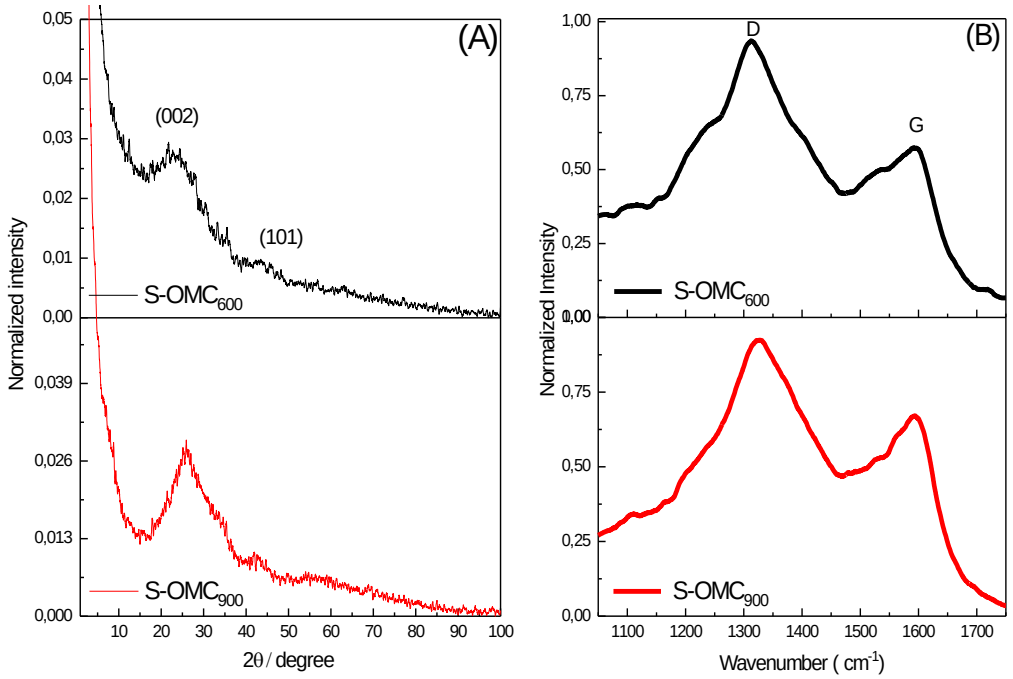

481

482 **Fig. S2.** (A) Wide-angle X-ray diffraction and (B) Raman of S-OMC$_{600}$ and OMC$_{900}$.

483

484

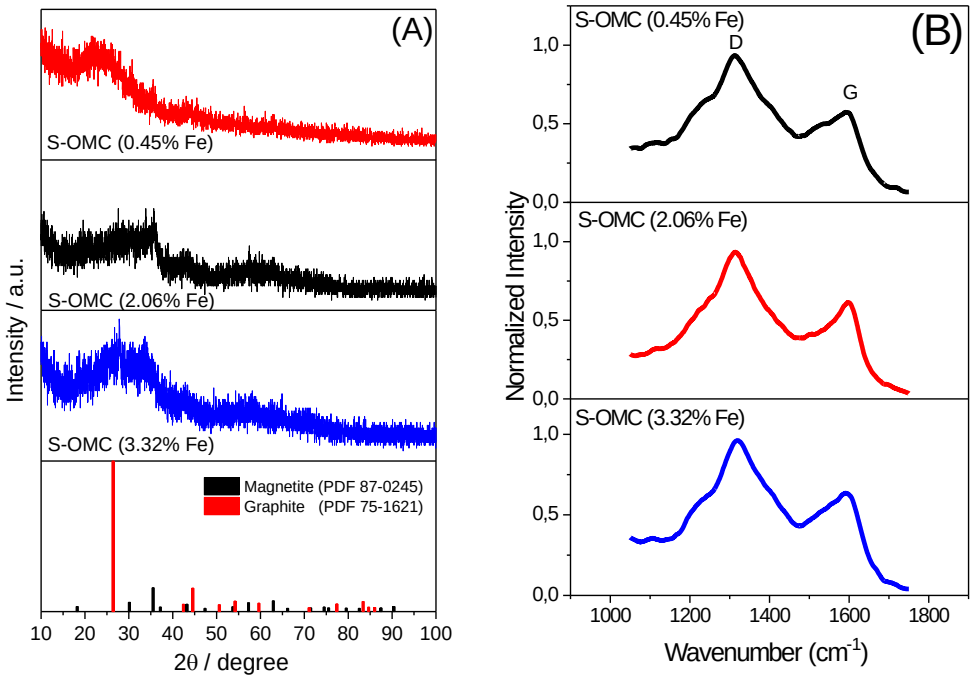

485

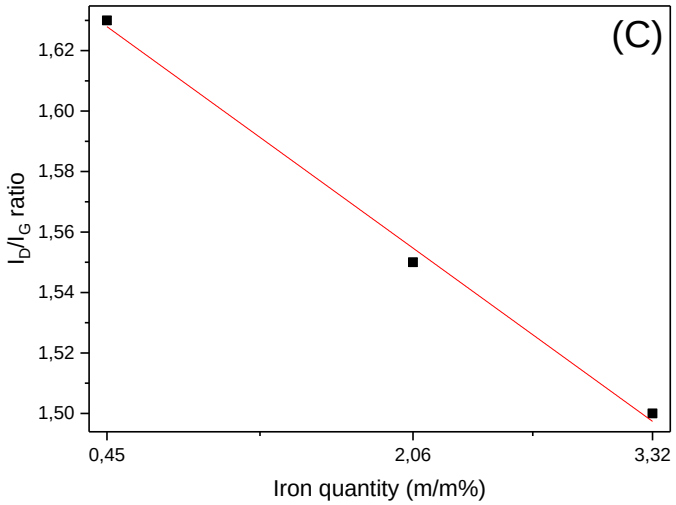

486

487 **Fig. S3.** Wide-angle X-ray diffraction (A) and Raman (B) of materials synthetized with

488 varying iron content. (C) Relation between the I_D/I_G and the iron quantity.

489

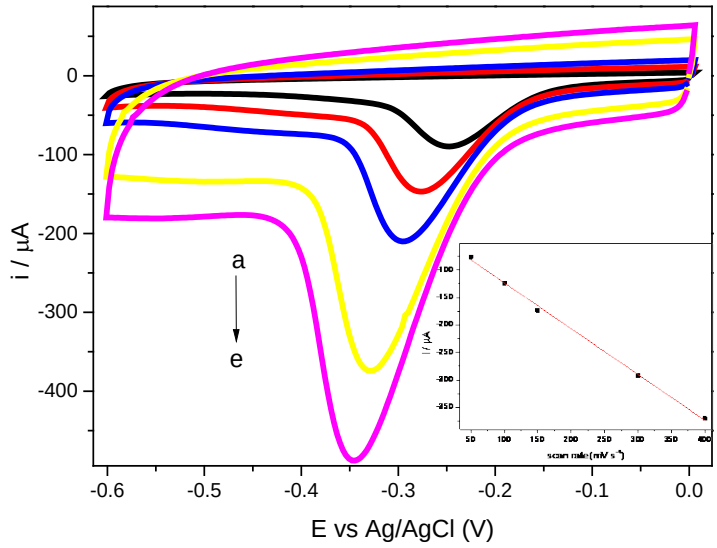

Fig. S4. Cyclic voltammetry of chloramphenicol using or S-OMC$_{900}$/GC as work electrode in 0.1 M H_2SO_4. From a to e, scan rate of 50, 100, 150, 300, 400 mV s^{-1}, respectively. Insets: Plots of i_{pc} versus scan rate.

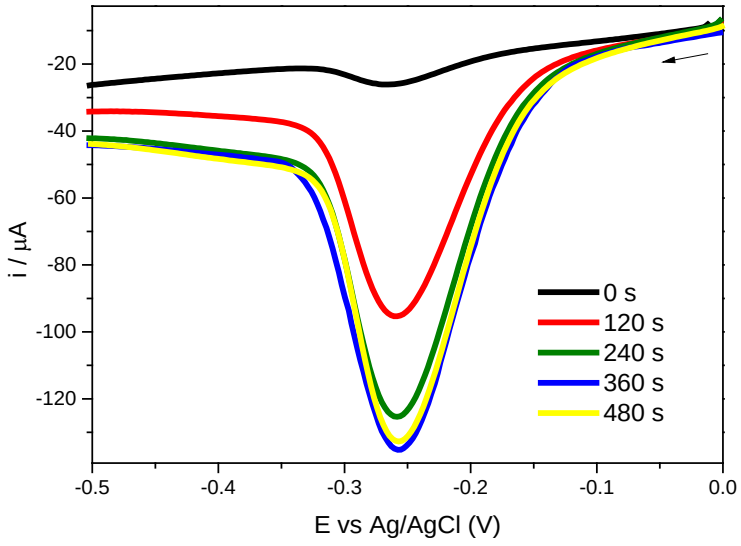

Fig. S5. LSV in H_2SO_4 0.1 M in presence of chloramphenicol with pre-concentration times of 0, 120, 240, 360 or 480 s under stirring.

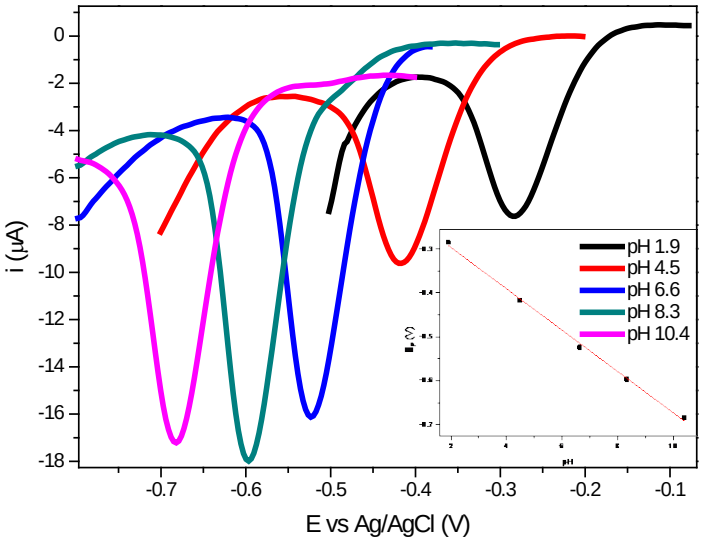

Fig. S6. LSV of chloramphenicol record with S-OMC$_{900}$/GC modified electrode in PBS at pH varying from 1.9 to 10.4. Inset: relation between the electrolyte pH and the peak potential.

Table S2. Electrochemical determination of chloramphenicol using different electrodes.

	Technique	Detection limit (mol L^{-1})	Electrode
[43]	LSV (540 s)	5.9 x10^{-7}	N-graphene / AuNP
[44]	DPV	7.4 x 10^{-8}	MIP/MWNT-AuNP
[48]	SWV	6 x 10^{-9}	Pretreated GC
[49]	DPV	2 x 10^{-9}	MIP-Carbon Paste
[50]	DPV	1.5 x 10^{-5}	3D-rGO
[51]	SWV	4.7 x 10^{-8}	Activated carbon fiber
[52]	SWV	4.7 x 10^{-8}	Carbon fiber
[53]	LSV (210 s)	2 x 10^{-8}	TiN-rGO
[54]	LSV (240 s)	8.5 x 10^{-9}	Nafion/OMC
This work	LSV (360 s)	7.9 x 10^{-9}	S-OMC

* LSV = linear sweep voltammetry; AuNP = Gold nanoparticle; DPV = differential pulse voltammetry; MIP = molecularly imprinted polymer; SWV = square wave voltammetry; MWCNT = multiwall carbon nanotube; TiN-rGO = Tetrapods-like titanium nitride–reduced graphene oxide.

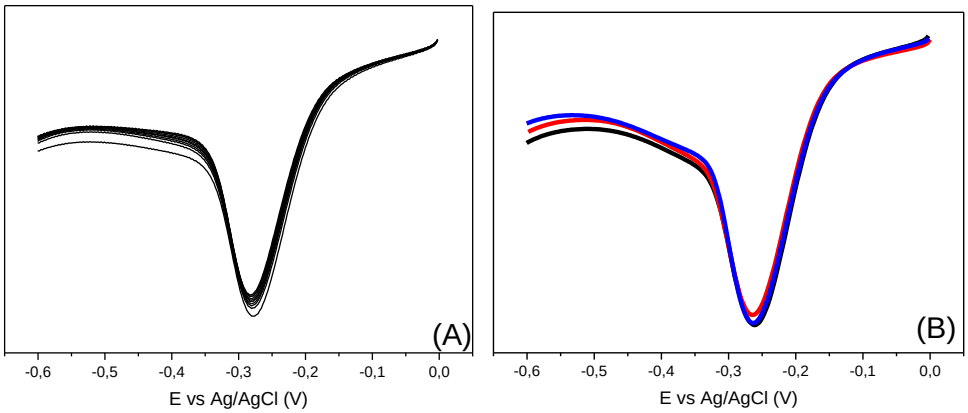

Fig. S7. Linear voltammetry in 0.1M H_2SO_4 in presence of 1.5 mM of chloramphenicol using (A) the same electrode ten times and (B) three freshly produced electrodes S-OMC_{900}.